IL NUOVO CIMENTO **45 C** (2022) 74
DOI 10.1393/ncc/i2022-22074-y

COMMUNICATIONS: SIF Congress 2021

# Lead-halide perovskite thin-film for flexible and direct X-ray detectors

M. VERDI([1])([2])

([1]) *INFN, Sezione di Bologna - Bologna, Italy*
([2]) *Dipartimento di Fisica e Astronomia (DIFA), Università di Bologna - Bologna, Italy*

received 15 February 2022

**Summary.** — Lead-halide hybrid perovskites are recently emerging as promising materials for high energy radiation detection thanks to the combination of high absorption coefficient, excellent transport properties, even in polycrystalline films, and their solution processability. Here we present flexible perovskite X-ray detectors based on solution deposited thin films. A triple cation perovskite is deposited on a thin plastic foil reaching no more than 3 $\mu$m in total thickness. Thanks to its small thickness, the detector can be adapted to very complex surfaces. The photodetector showed a clear and box-like response to 150 kVp X-ray with a sensitivity of $(6.30 \pm 0.02)$ $\mu\mathrm{CGy}^{-1}\mathrm{cm}^{-2}$ when operated in passive mode.

## 1. – Introduction

X and gamma ray detection is of extreme importance for a large number of applications ranging from crystallography to radio astronomy, including medical, industrial, public security and high energy physics applications. The largest demand for X-ray detectors comes from the medical field in which new, low cost, large area and flexible detectors are needed to improve real-time diagnostic techniques, such as the CT (computed tomography) and to unlock new functionality. Cancer is the second deadliest disease in the world after cardiovascular diseases. In 2020, 19.3 million new cancer cases and 10 million cancer deaths have been estimated by the International Agency for Research on Cancer [1]. In 2018, new cancer cases and deaths were 18.1 million and 9.6 million respectively, confirming the constant increase of cancer cases over the years [2]. Among the main instruments against cancer, ionizing radiations can be used for diagnostics and treatments. Driven by the increase of cases, the main goal of this research field is to find new materials for novel approaches to diagnosis, treatment and monitoring. The most promising material on the market for large area X-ray flat panel direct detectors is amorphous selenium ($\alpha$ -Se) which has a higher atomic number than silicon, but the cost

 

of which is high because of vacuum thermal deposition. $HgI_2$ and CZT are other interesting alternatives. However, the main problem of the first one is the large leakage current, while the second one is difficult to integrate with electronics due to the high temperature, high cost and limited dimensions of the single crystal fabrication [3, 4]. Moreover, the intrinsic stiffness and fabrication procedures do not allow their growth on flexible plastic substrates. Flexible or ultra-flexible X-ray detectors are desirable for different applications because they are lightweight, wearable and conformable to complex shapes, like the surface of the human body. For instance, in nuclear medicine it is important to monitor the doses delivered to patients. With an ultra-flexible detector, this study can be carried out in real-time in-situ directly on the patient skin. Another application could be in dental radiography, where a flexible detector capable of adapting itself to the complicated surface can improve the comfort of the patient during real-time radiography as well as spatial resolution. Mechanical flexibility, high X-ray sensitivity (up to $1.3 \times 10^4\,\mu\mathrm{CGy}^{-1}\mathrm{cm}^{-2}$) [5] and low limit of detection (down to $0.29\,\mu\mathrm{Gys}^{-1}$) [6] have been demonstrated for both organic single crystal and thin film direct X-ray detectors. Despite these encouraging results, organic semiconductors are intrinsically low-Z materials, therefore resulting in low high energy photon absorption. A solution to this problem can be the introduction of heavy elements in the form of nanoparticles inside the organic semiconductor film [7]. This approach is limited by the maximum nanoparticles concentration that can be dispersed in the organic semiconductor before clustering occurs, resulting in performance degradation. Recently, a new class of materials has attracted a lot of attention regarding ionizing radiation detection. Metallorganic lead-halide perovskites were demonstrated to be a great material for photovoltaic applications. Thanks to their exceptional optoelectronic properties, perovskite solar cells started in 2009 with a power conversion efficiency of 2.2% [8] and reached 25% and higher in just 12 years, making them the fastest-growing solar cell technology in history. The general chemical formula is $ABX_3$, in which A is an organic monovalent cation, B is a lead cation and X represents a halide atom (Cl, Br, I). Different combinations of organic cations and halide can be used; one of the interesting properties of these materials is the tunability of the electronic and optical properties by just varying the relative amount of the components inside the atomic structure. They are also good candidates for X-ray detectors for several reasons. First, the high X-ray attenuation coefficient, due to the presence of heavy elements in the perovskite structure, such as lead and iodine. A large carrier diffusion length makes it possible to fabricate films with good electronic properties. Third, high radiation hardness: these materials present a high deep defects formation energy that prevents the creation of trap levels, which are detrimental to the detector performances. Perovskites are solution-processable materials, both the fabrication of single crystals and thin polycrystalline films are possible at low temperatures ($<150\,^\circ\mathrm{C}$) from solution with common chemical facilities [9]. The low-temperature processability of these materials opens the possibility to large-area, low-cost and flexible X-ray detectors. However, there are few examples of perovskite thin-film flexible detectors [10]. Most of the works in literature are about perovskite single crystals that show extraordinary detection performance [11]. The very high performance of detectors based on single crystal can be ascribed to their thickness, ensuring high absorption, and to their good transport properties. Single crystal detectors suffer from the big problem of scalability, where the limiting factor is the maximum crystal area that can be grown. Thin film technology is instead ready to be scaled up, since industrial techniques for coating can be used also for depositing perovskite semiconductors. Moreover, the possibility to use plastic substrate will lead to the possibility of low-weight detectors, which are very appealing for space applications.

In this work, we present a flexible perovskite thin film X-ray detector with photodiode architecture. We fabricate flexible diodes on ultra-thin 1.3 $\mu$m thick PET foils making the full devices no more than 3 $\mu$m in thickness paving the way for high conformable X-ray detectors. The response of such a structure to 40 kVp X-rays has already been proved [12]. Here we studied the detector response to higher X-ray energies (150 kVp) compatible with the ones used in medicine during a CT scan.

## 2. – Results and discussion

We successfully fabricated an X-ray photodiode based on a hybrid lead-based perovskite with a p-i-n architecture on thin plastic foil. In this type of structure, the perovskite active layer is in the middle of it. For this work we used mixed-cation, mixed-halide, lead-based hybrid perovskite with chemical formula $Cs_{0.05}(FA_{0.83}MA_{0.17})_{0.95}PbI_{3-x}Br_x$ deposited from solution by spin coating (see method section). FA is the formamidinium cation and MA the methylammonium cation constituting the organic part of the perovskite. The perovskite layer, 500 nm thick, is interfaced with the hole and electron transport layer, see fig. 1(a). The hole transport layer (HTL) has the role to extract and transport the holes to the collecting electrode. The opposite for the electron transport layer (ETL), which has the role to bring the electrons to the collecting electrode. In our structure, we used as HTL a spin-coated layer of poly(3,4-ethylenedioxythiophene):poly(styrenesulphonate)(PEDOT:PSS). For the ETL we used N,N′-dimethyl-3,4,9,10-perylentetracarboxylic diimide (PTCDI). Both are organic semiconductors, the first is p-type and the second is n-type. For both interlayers, the deposited thickness is 100 nm. Between the ETL and the top gold contact, we deposited a thin layer (10 nm) of Chromium oxide ($Cr_2O_3$) which has good hole blocking capabilities and helps protect the gold from corrosive reaction with the perovskite [13]. The whole device is 3 $\mu$m thick and the 1.3 $\mu$m PET foil used as a substrate gives outstanding flexibility to the device. The picture in fig. 1(c) shows the ability to adapt itself to very complex surfaces, like wrinkles on a laboratory glove. In fig. 1(b), the measured current-voltage characteristic of the photodiode structure, in dark conditions, shows a very good rectification factor equal to $(1.5 \pm 0.2) \times 10^5$ calculated considering the current at $-1$ V and 1 V. In red the IV curve acquired after the exposure of the sample to 11 Gy of incident radiation with no significant degradation. In both IV curves, a small hysteresis is present, that can be ascribed to ion migration inside the perovskite layer.

We tested the performances of the detector under 150 kVp X-ray generated from a W-target tube. Figure 2(a) illustrates a simulated spectrum of the X-ray source used for this work. The fluxes have been calculated for a dose rate of 3000 $\mu$Gys$^{-1}$. The energies involved in this experiment are compatible with the ones used in medicine when performing a CT scan. We used a motorized lead shutter to modulate the X-ray beam impinging on the sample. We observed the change in current flowing through the device when irradiating with the X-ray. Figure 2(b) illustrates the detector response to repeated X-ray pulses under a constant dose rate equal to 5061 $\mu$Gys$^{-1}$ changing the applied bias. When the sample is exposed to the radiation it shows a clear and nice box-like response at all biases. The measured dark current, $(121 \pm 6)$ pA at 0 V, increases only slightly with the reverse bias, reaching $(2.4 \pm 0.2)$ nA at $-1$ V. The photodiode architecture has an intrinsic electric field produced at the interface of the perovskite layer with HTL and ETL. The internal electric field allows the extraction of the photogenerated charges at 0 V external bias. The dynamic response of the detector in passive mode (*i.e.*, no external bias applied) to different dose rates is displayed in fig. 2(c). Although a small shift in the

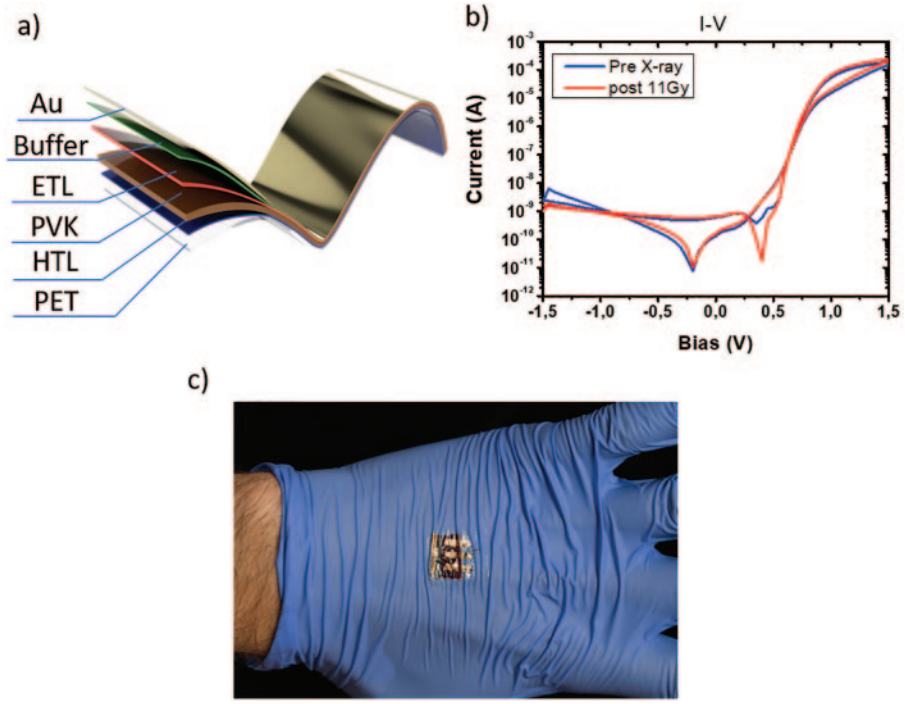


Fig. 1. – Ultraflexible photodiode detector. (a) The layered structure of a flexible perovskite-based photodiode with the p-i-n architecture. The substrate is a thin PET foil. In the center of the structure, the perovskite active layer is present. The perovskite is sandwiched between the hole and electron transport layers (HTL and ETL respectively). HTL and ETL have the role to extract and transport the photogenerated holes and electrons toward the electrodes. On top of the ETL, a buffer layer is usually deposited to improve the interface with the top metallic contact. (b) Current-Voltage characteristic (I-V) of an ultra-thin perovskite photodiode. In blue the IV acquired in dark conditions and in red the IV acquired in dark after the exposure to 11 Gy of incident X-ray, showing no degradation. (c) Picture of the ultraflexible X-ray detector placed on a glove. The picture shows the ability of the detector to follow very small curvature radii demonstrating the adaptability of the sensor to very complex surfaces.

dark current, $(35 \pm 5)$ pA between the first measurement at the lowest dose rate and the last one at the maximum dose rate, the perovskite photodetector shows an increasing photocurrent signal with increasing incident dose rate. The photocurrent is calculated as the difference between the current flowing in the device when the X-ray beam is on and the dark current. Working in passive mode could be interesting for wearable applications where low-consuming and low-voltage devices are very desirable, especially when the detector needs to be placed on the patient skin. Figure 2(d) demonstrates the linearity of the detector response to the radiation. For all the biases tested, the photocurrent extracted from the detector showed a linear behavior in the whole dose rate range. From these data it is possible to extract the sensitivity defined as the derivative of the signal produced by the detector and the dose rate, so $\frac{\partial S}{\partial D}$. Since in our case the relation is linear, we calculate the sensitivity as the slope of the line that best fits the data. The extracted sensitivity in passive mode resulted equal to $(6.30 \pm 0.02)\,\mu\mathrm{CGy}^{-1}\mathrm{cm}^{-2}$. The top sensitivity is reached at $-1$ V with a value of $(9.4 \pm 0.01)\,\mu\mathrm{CGy}^{-1}\mathrm{cm}^{-2}$. Despite

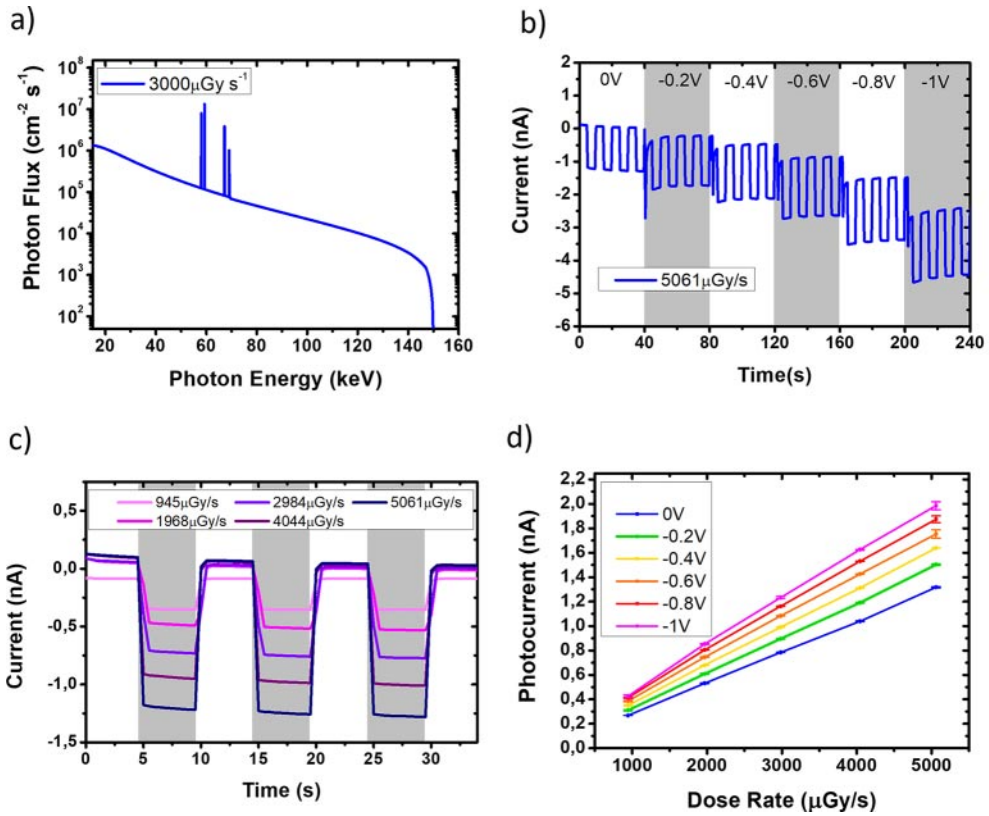


Fig. 2. – Detector response under 150 kVp. (a) Current response of the detector at constant incident dose rate with increasing external bias applied from 0 V to −1 V. The detector shows a box-like response when irradiated at all biases. The gray boxes help distinguish the different bias regions. (b) Dynamic response of the detector with 0 V external bias applied to different incident dose rates between 945 $\mu$Gys$^{-1}$ and 5061 $\mu$Gys$^{-1}$. The photodiode architecture combined with a very good quantum efficiency gives the possibility to work in passive mode maintaining a good performance. (c) Photocurrent *vs.* incident dose rate for the external bias applied. The detector presented a linear response for all the biases and a small increase of the slope with the increasing bias.

increasing the bias leads to a 49% increase in the sensitivity, the value obtained at 0 V is higher than others reported in the literature for devices with comparable perovskite thickness [14,15]. Moreover, the slight change in performances with the increasing reverse bias is a proof of the superior charge collection efficiency of our structure. In fact, we are able to collect most of the charges generated inside the perovskite layer with the intrinsic electric field of the junction.

## 3. – Conclusions

In this work we demonstrated the feasibility to use thin-film perovskite as an active layer in a photodiode architecture to fabricate an ultraflexible X-ray detector. The triple cation hybrid perovskite used for this work was deposited from solution by spin-coating.

The combination of the high absorption coefficient and excellent charge carrier collection efficiency, given by the p-i-n device structure, allows having a nice output signal even with a 500 nm perovskite layer. The top sensitivity $(9.4 \pm 0.01)\,\mu\mathrm{CGy}^{-1}\mathrm{cm}^{-2}$ was obtained by applying $-1$ V to the junction, but $(6.30 \pm 0.02)\,\mu\mathrm{CGy}^{-1}\mathrm{cm}^{-2}$ was measured in passive mode. We fabricated devices on a very thin plastic substrate giving the final detector unprecedented flexibility. Here we showed a linear, stable and repeatable response to 150 kVp X-ray beam demonstrating thin-film perovskite as a very good candidate for low-cost, large-area X-ray detector. Moreover, the possibility to fabricate devices at low temperature allows the fabrication of flexible detectors; thanks to the efficiency of the material, it is possible to employ this technology for wearable sensing applications where conformability, light-weight and low operating voltage are essential requirements.

## Appendix A.

### Materials and methods

A˙1. *Chemicals*. – The chemicals used for this work were purchased from commercial suppliers. Hellmanex III detergent (Hellma Analytics), Sylgard 184 Silicone Elastomer (PDMS, Dow Corning), PET foil (Mylar CW02), hexane (n-hexane, VWR, 98%), PEDOT:PSS aqueous dispersion (Clevios PH1000, Heraeus), Zonyl FS-300 (abcr GmbH), lead iodide (PbI2, Sigma Aldrich, 99.9%), lead bromide (PbBr2, Sigma Aldrich, 99.99%), cesium iodide (Sigma Aldrich, 99.9%), N,N-dimethylformamide (DMF, anhydrous, Sigma Aldrich), dimethylsulfoxide (DMSO, VWR, 99.5%), isopropanol (2-propanol, reagent grade), N,N′-dimethyl-3,4,9,10-perylentetracarboxylic diimide (PTCDI, purified through sublimation 2 times, Hoechst). Methylammonium bromide (MABr) was synthesized from methylamine [33 weight% (wt%) in absolute ethanol; Sigma Aldrich] and hydrobromic acid (HBr, 48 wt%, aqueous; Sigma Aldrich) and purified using diethylether (VWR) and absolute ethanol (Merck Millipore). Methylammonium iodide (MAI) and formamidinium iodide (FAI) were synthesized using analogous procedure using hydroiodic acid (HI, 57 wt%, aqueous; Sigma Aldrich).

A˙2. *Solutions*. – The PDMS solution was prepared by mixing 1:10 w/w of cross-linker to hardener and then diluting it 1:1 w/w with hexane.

The PEDOT:PSS solution was prepared by mixing Clevios PH1000 stock solution with 5 vol% DMSO and 0.5 vol% Zonyl FS-300, stirring at room temperature for an hour and keeping at 4 °C overnight. The PEDOT:PSS solution was filtered through Minisart RC25 Syringe filter 0.45 $\mu$m regenerated cellulose right before use.

Perovskite solution ($Cs_{0.05}$ $(FA_{0.83}MA_{0.17})_{0.95}PbI_{3-x}Br_x$) was prepared by mixing PbI2 (507.5 mg, 1.10 mmol), FAI (172 mg, 1.00 mmol), MABr (22.4 mg, 0.20 mmol), and PbBr2 (73.5 mg, 0.20 mmol) in 1 mL of DMF and DMSO (4:1 v/v ratio, respectively) followed by stirring at 45 °C until dissolved. Afterwards, CsI (0.063 mmol, from 1.5 M stock solution in DMSO) was added to the mixture and stirred overnight. The solution was filtered using polytetrafluoroethylene (PTFE) syringe filters (0.45 $\mu$m; Whatman) before spin-coating.

A˙3. *Photodiode fabrication*. – Glass substrates (1.5 cm × 1.5 cm, 1 mm thick) were cut and cleaned in an ultrasonic bath for 30 min each in 2 v/v% Hellmanex in DI water solution, 2× DI water solution, isopropanol, and dried using $N_2$. Then The PDMS solution was spin-coated at 4000 rpm for 30 s on glass and placed on a heat plate at 150 °C for 10 min to cross-link. Next, the 1.3 $\mu$m The PET foil was carefully placed on the sample avoiding air pockets and then transferred to a heating plate again at

110 °C for other 10 min. Afterwards, C/rAu (10/100 nm) bottom contacts were thermally evaporated (0.1–1 nm $s^{-1}$ at base pressure $1 \times 10^3$ mbar). The PEDOT:PSS solution was spin-coated at 1500 rpm for 45 s followed by 1000 rpm for 2 s (ramp 1 s) and annealed at 122 °C for 15 min. Then the film was washed by spin-coating isopropanol solution at 1500 rpm for 4 s followed by 4000 rpm for 12 s and annealed at 120 °C for 15 min. For further deposition of the perovskite layer, the samples were transferred into $N_2$ glovebox. The perovskite solution was deposited using an anti-solvent procedure. The solution was spin-coated in two steps at 1500 rpm for 10 s followed by 6000 rpm for 30 s. Approximately 0.2 mL of chlorobenzene (anti-solvent) was dropped for about 3 s. Then the film was annealed at 100 °C for 1 h.

The PTCDI layer (100 nm) was deposited onto the sample via thermal evaporation at 0.5–2 nm $s^{-1}$ rate and base pressure $1 \times 10^3$ mbar. This was followed by the thermal evaporation of Cr/Au contacts (10/100 nm) at rate of 0.1–1 nm $s^{-1}$ and base pressure $1 \times 10^3$ mbar.

A˙4. *Device characterization under X-rays.* – Electrical characterization of the samples under X-ray irradiation was performed in a $N_2$-filled Faraday box with a 70 $\mu$m front Al window. As X-ray source a Hamamtsu L12161 X-ray tube with tungsten target was used at fixed 150 kV operating voltage and the filament current was changed between 100 and 500 $\mu$A leading to an incident dose rates on the sample between 945 and 5061 $\mu Gys^{-1}$. The dose rate calibration was previously performed employing the Barracuda radiation detector (RTI Group). The modulation of the beam was obtained with a homemade mechanical lead shutter placed close to the X-ray tube window. Keithley SMU 2614 was used in combination with a LabVIEW program for electrical signal acquisition.

* * *

The author acknowledges the Semiconductor Physic group of the University of Bologna directed by Beatrice Fraboni. Martin Kaltenbrunner, Niyazi Serdar Sariciftci and Markus Clark Scharber for their hospitality and the resources provided. The author also acknowledges Laura Bariscó, Andrea Ciavatti, Stepan Demchyshyn and Bekele Hailegnaw for their help and precious advice during the work.

REFERENCES

[1] Sung H., Ferlay J., Siegel R. L., Laversanne M., Soerjomataram I., Jemal A. and Bray F., *Cancer J. Clin.*, **71** (2021) 21660.
[2] Bray F., Ferlay J., Siegel R. L., Laversanne M., Soerjomataram I. and Jemal A., *Cancer J. Clin.*, **68** (2018) 21492.
[3] Kabir M. Z., Yunus M., Kasap S. O., Tousignant O., Mani H. and Gauthier P., *Curr. Appl. Phys.*, **6** (2006) 393.
[4] Kasap S. and Capper P., *Springer Handbook of Electronic and Photonic Materials* (Springer) 2017.
[5] Temiño I., Basiricó L., Fratelli I., Tamayo A., Ciavatti A., Mas-Torrent M. and Fraboni B., *Nat. Commun.*, **11** (2020) 2136.
[6] Zhao D., Xu M., Xiao B., Zhang B., Yan L., Zeng G., Dubois A., Sellin P., Jie W. and Xu Y., *J. Mater. Chem. A*, **8** (2020) 5217.
[7] Thirimanne H. M., Jayawardena K. D. G. I., Parnell A. J., Bandara R. M. I., Karalasingam A., Pani S., Huerdler J. E., Lidzey D. G., Tedde S. F., Nisbet A., Mills C. A. and Silva S. R. P., *Nat. Commun.*, **9** (2018) 2926.
[8] Kojima A., Teshima K., Shirai Y. and Miyasaka T., *J. Am. Chem. Soc*, **131** (2009) 6050.

[9] Basiricó L., Ciavatti A. and Fraboni B., *Adv. Mater. Technol.*, **6** (2021) 2000475.
[10] Lédée F., Ciavatti A., Verdi M., Basiricó L., Fraboni B., *et al.*, *Adv. Opt. Mater.*, **14** (2021) 2101145.
[11] Wei H., Fang Y., Mulligan P., Chuirazzi W., Fang H. H., Wang C., Ecker B. R., Gao Y., Loi M. A., Cao L. and Huang J., *Nat. Photon.*, **10** (2016) 333.
[12] Demchyshyn S., Verdi M., Basiricó L., Ciavatti A., Hailegnaw B., Cavalcoli D., Scharber M. C., Sariciftci N. S., Kaltenbrunner M. and Fraboni B., *Adv. Science*, **7** (2020) 2002586.
[13] Kaltenbrunner M., Adam G., Glowacki E. D., Drack M., Schwödiauer R., Leonat L., Apaydin D. H., Groiss H., Scharber M. C., White M. S., Sariciftci N. S. and Bauer S., *Nat. Mater*, **14** (2015) 4388.
[14] Yakunin S., Sytnyk M., Kriegner D., Shrestha S., Richter M., Matt G. J., Azimi H., Brabec C. J., Stangl J., Kovalenko M. V. and Heiss W., *Nat. Photon.*, **9** (2015) 444.
[15] Basiricó L., Senanayak S. P., Ciavatti A., Abdi-Jalebi M., Fraboni B. and Sirringhaus H., *Adv. Funct. Mater.*, **29** (2019) 1902346.